JOURNAL OF SPACECRAFT AND ROCKETS
Vol. 45, No. 5, September–October 2008

Spectrum Modeling for Air Shock-Layer Radiation at Lunar-Return Conditions

Christopher O. Johnston* and Brian R. Hollis†
NASA Langley Research Center, Hampton, Virginia 23681
and
Kenneth Sutton‡
National Institute of Aerospace, Hampton, Virginia 24060

DOI: 10.2514/1.33004

A new air-radiation model is presented for the calculation of the radiative flux from lunar-return shock layers. For modeling atomic lines, the data from a variety of theoretical and experimental sources are compiled and reviewed. A line model is chosen that consists of oscillator strengths from the National Institute of Standards and Technology database and the Opacity Project (for many lines not listed by the National Institute of Standards and Technology), as well as Stark broadening widths obtained from the average of available values. Uncertainties for the oscillator strengths and Stark broadening widths are conservatively chosen from the reviewed data, and for the oscillator strengths, the chosen uncertainties are found to be larger than those listed in the National Institute of Standards and Technology database. This new atomic line model is compared with previous models for equilibrium constant-property layers chosen to approximately represent a lunar-return shock layer. It is found that the new model increases the emission resulting from the 1–6-eV spectral range by up to 50%. This increase is due to both the increase in oscillator strengths for some important lines and to the addition of lines from the Opacity Project, which are not commonly treated in shock-layer radiation predictions. Detailed theoretical atomic bound–free cross sections obtained from the Opacity Project's TOPbase are applied for nitrogen and oxygen. An efficient method of treating these detailed cross sections is presented. The emission from negative ions is considered and shown to contribute up to 10% to the total radiative flux. The modeling of the molecular-band systems using the smeared-rotational-band approach is reviewed. The validity of the smeared-rotational-band approach for both emitting and absorbing-band systems is shown through comparisons with the computationally intensive line-by-line approach. The absorbing-band systems are shown to reduce the radiative flux by up to 10%, whereas the emitting-band systems are shown to contribute less than a 5% increase in the flux. The combined models chosen for the atomic line, atomic bound–free, negative-ion, and molecular-band components result in a computationally efficient model that is ideal for coupled solutions with a Navier–Stokes flowfield. It is recommended that the notable increases shown, relative to previous models, for the atomic line and negative-ion continuum should be included in future radiation predictions for lunar-return vehicles.

Nomenclature

B_e	=	Klein–Dunham coefficient
b_v	=	line-shape function
c	=	velocity of light, 2.997925×10^{10} cm/s
E_J	=	rotational term energy for a molecule, cm^{-1}
E_V	=	vibrational term energy for a molecule, cm^{-1}
E_e	=	electronic term energy for a molecule, cm^{-1}
E_i	=	electronic term energy for an atomic level i, cm^{-1}
E_{ionize}	=	ionization energy of an atomic level i
E_u	=	energy of the upper electronic level for a bound–bound transition
e	=	electron charge, 4.80298×10^{-10} $\text{cm}^{3/2}\,\text{g}^{1/2}/\text{s}$
f_{ij}	=	atomic line oscillator strength for a lower level i and upper level j
g_i	=	degeneracy for an atomic level i
g_x	=	degeneracy of the molecular energy mode x, with x being either J, V, or e
h	=	Planck's constant, 6.6256×10^{-27} erg · s
j_v	=	frequency-dependent emission coefficient, $\text{erg}/\text{cm}^3 \cdot \text{sr}$
k	=	Boltzmann constant, 1.38054×10^{-16} erg/K
m	=	electron mass, 9.1091×10^{-28} g
N_a	=	number density of an atom a, $\text{particles}/\text{cm}^3$
N_i	=	number density of an atomic level i, $\text{particles}/\text{cm}^3$
N_e	=	number density of electrons or of a molecular electronic state, $\text{particles}/\text{cm}^3$
N_+	=	ion number density, $\text{particles}/\text{cm}^3$
Q_x	=	partition function of energy mode x, with x being either J, V, or e
q-cumulative	=	spectrally running total of the radiative heat flux starting at 0 eV, W/cm^2
q_{hv}	=	frequency-dependent (in terms of electron volts) radiative heat flux, $\text{W}/\text{cm}^2/\text{eV}$
T_x	=	temperature of energy mode x (with x being either J, V, or e), K
V	=	vibrational quantum number
w	=	wave number, cm^{-1}, $1/\lambda$ or v/c
$\Delta\lambda_S$	=	Stark broadening full width at half-height, nm
$\Delta\lambda_{S,0}$	=	Stark broadening coefficient, $\Delta\lambda_S$ at 10,000 K and $N_e = 1 \times 10^{16}$ $\text{particles}/\text{cm}^3$
Δz	=	thickness of a constant-property slab, cm
λ	=	wavelength, nm
v	=	frequency, s^{-1}

Received 22 June 2007; revision received 18 April 2008; accepted for publication 28 April 2008.

*Aerospace Engineer. Member AIAA.
†Aerospace Engineer. Senior Member AIAA.
‡Senior Research Fellow. Associate Fellow AIAA.

Subscripts

CL	=	indicates the centerline in the spectrum of an atomic or molecular line
e	=	refers to the electronic energy mode
EQ	=	assumes that Boltzmann–Saha equilibrium exists among the electronic levels
$h\nu$	=	indicates a spectral dependence in terms of electron volts ($1.24 \times 10^{-4}\nu/c$)
i	=	refers to the lower electronic state of an atomic transition
j	=	refers to the upper electronic state of an atomic transition
V	=	refers to the vibrational energy mode
ν	=	indicates frequency dependence

Superscripts

$-$	=	indicates a negative ion
$'$	=	defines a value in the upper electronic state of a molecular transition
$''$	=	defines a value in the lower electronic state of a molecular transition

I. Introduction

RENEWED interest in lunar and Mars return has initiated studies of the aerothermal environments produced around the vehicles used for such missions. This requires, among other challenges, the prediction of the radiative flux to the vehicle from the shock-layer gas. Although experimental data are available for validating these prediction models in the infared (IR) region of the spectrum [1], there is essentially no data for the equally important vacuum ultraviolet (VUV) region. Furthermore, comparisons of the available IR data with a preliminary version of the model presented in this paper [2] and an updated version of the NEQAIR code [3] have indicated a 10–20% underprediction of the measurements. Other comparisons between various experimental data and various radiation models have provided no better agreement. Therefore, to increase the confidence in both the IR and VUV shock-layer radiation predictions, an assessment of the relevant data available for high-temperature air-radiation modeling is needed. Both a review of the data applied in previous models, which are discussed in the following paragraph, and a compilation of recently available data are required for this purpose. In addition, a computationally efficient method of applying these data is of interest for applications such as coupling the radiation model with a flowfield solver.

The three main codes that have provided the majority of the shock-layer radiative heating predictions at NASA over the past 35 years are the RAD/EQUIL, NEQAIR, and LORAN codes. The earliest of these, which is referred to in the literature as either RAD/EQUIL, RAD, or RADICAL, was developed by Nicolet [4]. This code modeled the spectral shape of each atomic line based on the atomic line data compiled by Wilson and Nicolet [5]. Not all of the atomic lines listed by Wilson and Nicolet were treated individually in the code. To reduce computational time, lines spaced closely in the spectrum were combined into composite lines, and weak lines were ignored. The atomic continuum and molecular bands were modeled as smooth curve fits, similar to those presented by Hoshizaki and Wilson [6]. The radiative heating prediction capability of RAD/EQUIL was developed assuming chemical and thermodynamic equilibrium. The second significant radiation code, NEQAIR, avoids this equilibrium assumption by applying a collisional-radiative, or non-Boltzmann, model. This code was developed by Park [7,8] and was based on the original code by Whiting et al. [9]. The atomic line data complied by Wiese et al. [10] and Griem [11] were applied in the original version of this code. Nearly 4 times more lines were treated in NEQAIR than in RAD/EQUIL. The molecular-band systems were modeled in NEQAIR using the line-by-line approach presented by Arnold et al. [12]. This is a significant difference between NEQAIR and RAD/EQUIL because of the large computational cost of applying the line-by-line approach relative to RAD/EQUIL's approximate curve-fit approach for the molecular-band systems. As an alternative to the RAD/EQUIL and NEQAIR codes, Chambers [13] developed the code LORAN, which is composed essentially of the atomic spectral model and quasi-steady-state model of NEQAIR along with a smeared-rotational-band (SRB) model for the molecular bands. This avoids the computationally intensive line-by-line molecular-band computation applied in NEQAIR. A comparison of the LORAN and NEQAIR results was presented by Hartung [14], who showed that the two codes predicted wall radiative-flux values that differed by only 6% for the cases considered.

In the time since the development of the RAD/EQUIL, NEQAIR, and LORAN codes, new data for atomic line, atomic photoionization, and molecular-band radiation has become available. The purpose of this paper is to determine the influence of this new data on the radiative heating emitted from lunar-return shock layers ($8000 < T < 11,000$ K and $0.1 < p < 1.0$ atm). Furthermore, a new radiation model is proposed in this paper based on this new data. This model is developed with the intention of applying it to nonequilibrium chemistry, multiple temperature, and non-Boltzmann conditions [15]. The ability to treat these nonequilibrium conditions is achieved by formulating the emission *and* absorption coefficient as a function of each radiative transition's upper and lower electronic state number density, respectively. Johnston [15] addresses the problem of calculating the number densities of the atomic and molecular electronic states required for this non-equilibrium radiation calculation. For the examples worked in the present paper, the assumptions of chemical equilibrium and Boltzmann electronic state populations are applied. Although these assumptions are restrictive, they are relevant to many of the shock-layer conditions of present interest [3]. The convenience of these assumptions is that they allow the number densities of the flowfield species to be determined by specifying only the temperature and pressure of the gas. The equilibrium chemical compositions applied in this work are obtained from the code developed by Prabhu and Erickson [16].

A simplified model of a shock-layer flowfield is treated throughout this study to make clear the influences of the strongly emitting inviscid region and the strongly absorbing boundary layer. This model, which is shown in Fig. 1, consists of two constant-property layers (which extend infinitely in the vertical direction) of equilibrium air at the same pressure, but at different temperatures (T_1 and T_2) and with different thicknesses (Δz_1 and Δz_2). The inviscid region of the layer is modeled with layer 1 and the boundary layer is modeled with layer 2. The equivalent of the wall-directed radiative flux at the edge of the boundary layer (layer 1) is q_1 and at the wall (layer 2) is q_2. To model the stagnation line of an Apollo-like vehicle at peak heating (see Fig. 1 of [2]), the required parameters are listed as cases 1 and 2 in Table 1. Case 1 consists of only layer 1 and will be studied extensively throughout this paper to compare the emission from various models. Case 2 consists of layer 1, which is the same as in case 1, as well as lower temperature and thinner layer 2. Also listed in Table 1 are cases 3 and 4, which will be discussed in Sec. VII. Note that the radiative flux from these constant-property (tangent-slab) layers is calculated throughout this paper using the improved exponential integral approximations presented in Appendix F of [15].

To begin the discussion of the radiation model developed in this paper, the radiative properties of atomic nitrogen and oxygen are discussed in Sec. II. The atomic line models for these species are compiled, including the Stark broadening half-widths, based on

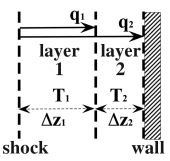

Fig. 1 Layout and definition of the double-layer case treated throughout this study.

Table 1 Case definitions for the double-layer problem defined in Fig. 1

Case ID	p, atm	T_1, K	Δz_1, cm	T_2, K	Δz_2, cm
1	0.5	10,000	15.0	——	——
2	0.5	10,000	15.0	5000	1.0
3	0.5	8000	15.0	——	——
4	1.0	15,000	0.8	8000	0.4

atomic data from various experimental and theoretical sources. The uncertainties of the oscillator strengths and Stark broadening half-widths are estimated from an extensive review of available data. The results of the compiled atomic line model are compared with the result of previous models. Details of the numerical treatment of the atomic lines are discussed in Sec. III, which focuses on the layout of the spectral grid. The atomic bound–free photoionization contribution is reviewed in Sec. IV, with a final model being developed based on data from the TOPbase database [17]. The treatment of the negative-ion continuum is discussed in Sec. V, and Sec. VI discusses the implementation of the SRB method for calculating molecular-band radiation. Sec. VII applies the models developed throughout this paper to equilibrium conditions relevant to lunar-return shock layers and provides a summary of the contributions from each of the discussed radiation mechanisms. Comparisons between the present model and the RAD/EQUIL code, which has been applied in many previous shock-layer radiation studies [18–22] and engineering correlations [23,24], are presented in each section for reference.

II. Assembling Data for Atomic Line Radiation

The primary source of atomic line data for the present study was the National Institute of Standards and Technology (NIST) atomic line database [25], compiled by Wiese et al. [26] in 1996. This database contains a comprehensive list of atomic line data for nitrogen and oxygen atoms, along with many others. The wavelengths and energy levels contained in this list are experimental values from Moore [27] and Kelly [28], which are well known with uncertainties of less than 0.001% [29]. The NIST values for the absorption oscillator strengths f_{ij} are from a combination of experimental [30–34] and theoretical [35,36] sources. For the lines with both experimental and theoretical data available, Wiese et al. [26] applied the average of these values. For many of the weaker lines, only the theoretical results from the Opacity Project (OP) [35] were available, which Wiese et al. [26] used directly. The Opacity Project is a completely theoretical atomic line database that contains many lines not contained in the NIST database, although only multiplet data, and not individual line data, are listed. These additional lines are mostly those with upper-level principal quantum numbers greater than 6, which were intentionally omitted from the NIST database because their accuracy was considered poor [26]. For the present model, the line data from the NIST database are applied for all lines contained in that database, whereas for lines not in the NIST database but included in the OP database, the OP multiplet data are applied. This results in 263 and 176 line multiplets, which contain 1082 and 842 individual lines, from the NIST database for nitrogen and oxygen, respectively. In addition, the 2190 and 2274 line multiplets from the OP database, which are those that do not repeat the NIST lines, are also applied. These OP lines are not separated into individual lines because they are mostly optically thin and because the data are not available. Furthermore, 99% of the OP line contribution comes from the strongest 500 multiplets (ranked in terms of their optically thin emission), which allows for a significant reduction in the number of OP lines required.

The influence of the additional OP multiplets is indicated in Fig. 2, which compares the radiative intensity, accounting for only the nitrogen line emission and absorption resulting from case 1 (defined in Table 1): in other words, a 15-cm constant-property layer of equilibrium air at a temperature of 10,000 K and a pressure of 0.5 atm. The line broadening applied in this comparison is presented later in this section. The "Wiese et al. (1996)" label refers to the NIST

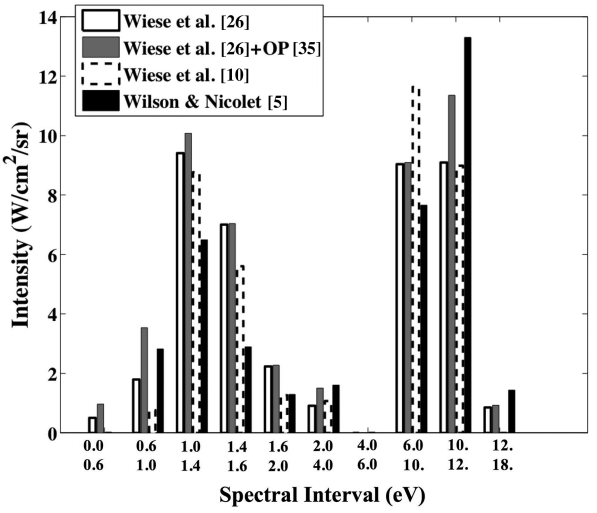

Fig. 2 Comparison of the intensity from an equilibrium slab of air, assuming emission and absorption from only nitrogen atomic lines, between various line models.

lines alone and the "Wiese et al. (1996) + OP" label refers to the combination of the NIST lines and the additional OP lines. From the difference between these values in each spectral range, it is seen that the OP lines contribute noticeably in the 0–1-eV range, as well as the 10–12-eV range, with the total increase from the OP lines being 6 $\mathrm{W/cm^2/sr}$ (or 15.3%), which is the cumulative effect of the large number of weak OP lines (meaning that there are not just a few OP lines that provide the majority of this increase). As will be shown in Sec. IV, these two spectral ranges have the largest contribution from the atomic bound–free mechanism, which is produced by transitions between bound electronic states and an ionized state. The OP lines are the result of transitions between two bound electronic states, although the upper state is very near the ionization limit. Thus, these lines should be located near the photoionization edges, which is where the bound–free emission is the strongest. Armstrong [37] showed that these lines could be treated approximately by shifting the photoionization edges by roughly 0.15 eV. The result of this approximate approach, which is applied in the RAD/EQUIL code, is presented in Sec. IV.

Also shown in Fig. 2 are the results of the older Wiese et al. [10] and Wilson and Nicolet [5] line models (obtained by applying both their oscillator strength and Stark broadening data), which were applied in the RAD/EQUIL [4] and original NEQAIR [7] codes, respectively. These models are seen to be generally weaker in the 0–6-eV range and stronger in the 6–12-eV range, compared with the Wiese et al. [26] model. Note that RAQ/EQUIL applies the photoionization edge shift, as mentioned previously, to account for line upper levels near the ionization limit. This contribution is not included in the Wilson and Nicolet [5] results shown in Fig. 2. Also not included in the Wilson and Nicolet [5] results is the pseudo-continuum that they apply in the 0–1-eV range to account for lines with both upper and lower levels near the ionization limit [38], which is why no line contribution is shown for Wilson and Nicolet [5] in the 0–0.6-eV range. For the present case, the pseudocontinuum contributes 0.8 $\mathrm{W/cm^2/sr}$ in the 0–1-eV range. To see the differences between the spectrally integrated radiative-flux values produced by the various line models, Fig. 3 presents the cumulative radiative flux resulting from the emission of nitrogen atomic lines and absorption from all radiative mechanisms.

To assess the Wiese et al. [26] oscillator strength data applied in the present model, these values were compared with those from various other sources for the strongest lines of nitrogen and oxygen. The strongest line multiplets were selected by determining the largest contributors to the radiative intensity for the constant-property case from Figs. 2 and 3. These multiplets are listed in Table 2 for nitrogen and in Table 3 for oxygen (note that none of the included OP lines are strong enough for inclusion on these lists). For nitrogen, although the

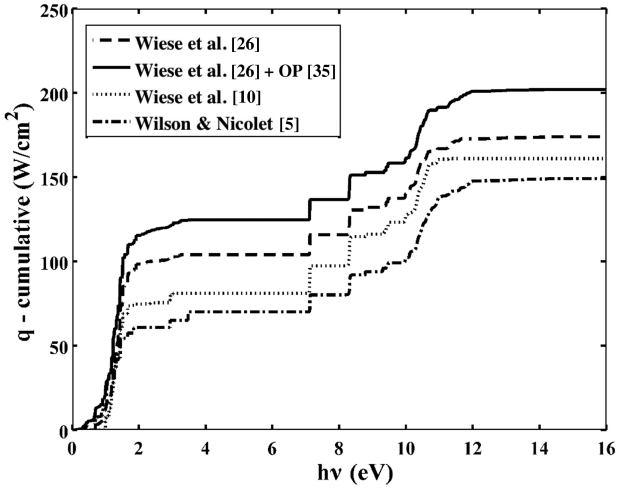

Fig. 3 Comparison of the cumulative radiative flux from an equilibrium slab of air between various line models, assuming emission from only nitrogen atomic lines and absorption from all radiative mechanisms.

33 chosen multiplets contain only 147 of the total 1082 individual lines listed by Wiese et al., they contribute roughly 75% of the total line flux for case 1. The various theoretical and experimental oscillator strength values available in the literature were compiled for these lines. Figures 4 and 5 present these values, which are normalized by the Wiese et al. data from 1996 (this is the only source that provides a value for each of these lines), for the VUV and IR lines, respectively. The Wiese et al. oscillator strengths f_{ij} are listed in Table 2. The Wiese and Fuhr [39] values from 2007, which are based entirely on the theoretical results of Fischer and Tachiev [40], and the Tayal [41] values from 2006 are the most recent theoretical results presented in this comparison. The older theoretical results of Hibbert et al. [36] and Wilson and Nicolet [5] are shown for reference and because the newer theoretical results are not available for many of the VUV lines. Also, the Wilson and Nicolet values, as well as the Wiese et al. [10] values from 1966 have been applied extensively in previous shock-layer radiation calculations. The experimental values from Goldbach et al. [30–32], Dumont et al. [42], and Hutchinson [43] are shown for the VUV multiplets in Fig. 4, and those from Musielok et al. [34], and Zhu et al. [33] are shown for the IR multiplets in Fig. 5. Ignoring the older Wilson and Nicolet [5] and Wiese et al. [10] values, the agreement between the various experimental and theoretical results is relatively good, although not as good as the published uncertainties by Wiese et al. [26] suggest. Therefore, new uncertainties are presented in Table 2 based on the deviation of the post-1970 data (therefore neglecting the Wiese et al. [10] and Wilson and Nicolet [5] data) shown in Figs. 4 and 5 from the Wiese et al. [26] values. For the multiplets with only the Wilson and Nicolet [5] values to compare with the Wiese et al. [26] data (multiplets 1, 2, 4, and 5), the Wilson and Nicolet [5] data were used in the uncertainty determination. These new uncertainties are generally higher than those proposed by Wiese et al. [26], although a few remain the same. A minimum uncertainty of 10% was chosen because no experimental measurements contain an uncertainty lower than this value. The uncertainties listed in Table 3 for oxygen lines are taken directly from Wiese et al. [26].

In addition to the oscillator strength and electronic level data required for the modeling of each individual atomic line, the Stark

Table 2 Summary of the strongest nitrogen line multiplets

ID no.	Wiese 96 ID[a]	No. of lines	$h\nu$, eV	$\lambda_{CL,mult}$, nm	i[b]	j	f_{ij}	f_{ij} % uncertainty	$\Delta\lambda_{S,0}$, nm	$\Delta\lambda_{S,0}$ % uncertainty	Wiese 66 ID[c]	Wilson 67 ID[d]
1	24	3	11.61	106.80	2	30	8.43e − 3	75	9.79e − 3	75	——	76
2	23	3	11.29	109.77	2	28	1.61e − 2	75	5.70e − 3	75	——	71
3	19	3	10.62	116.79	2	18	3.69e − 2	50	7.88e − 4	40	9	63
4	17	3	10.53	117.69	2	15	1.28e − 2	50	9.19e − 4	40	14	59
5	39	3	10.42	118.91	3	30	8.76e − 3	75	1.21e − 2	75	——	58
6	38	4	10.41	119.10	3	30	4.65e − 3	75	1.08e − 2	75	——	57
7	1	3	10.33	120.00	1	4	2.59e − 1	20	1.28e − 4	50	2	56
8	37	3	10.12	122.52	3	28	1.65e − 2	75	7.10e − 3	75	——	55
9	16	4	9.972	124.32	2	13	7.96e − 2	20	1.84e − 4	100	5	53
10	35	3	9.459	131.07	3	21	3.64e − 2	60	7.36e − 4	30	13	52
11	32	4	9.396	131.95	3	16	2.18e − 2	20	7.50e − 4	30	11	51
12	30	3	8.781	141.19	3	13	2.56e − 2	20	2.52e − 4	100	6	49
13	15	3	8.302	149.33	2	5	7.15e − 2	10	2.97e − 4	30	3	48
14	29	4	7.110	174.36	3	5	3.69e − 2	20	3.46e − 4	50	4	47
15	48	3	1.663	745.42	4	10	1.05e − 1	10	8.94e − 3	30	23	35
16	47	7	1.509	821.41	4	9	3.14e − 1	10	8.93e − 3	30	22	33
17	52	4	1.438	861.98	5	12	3.51e − 1	10	1.38e − 2	30	25	32
18	46	8	1.426	869.40	4	8	4.66e − 1	15	9.17e − 3	30	21	31
19	65	2	1.369	905.24	7	16	1.10e + 0	25	3.95e − 2	30	33	30
20	127	3	1.369	905.01	13	28	4.80e − 1	15	3.08e − 2	30	27	——
21	126	4	1.347	919.82	13	28	3.31e − 1	50	2.50e − 1	100	——	——
22	51	3	1.319	939.79	5	11	5.81e − 1	25	1.42e − 2	50	24	29
23	72	10	1.260	983.33	8	20	1.36e − 1	15	3.71e − 2	50	35	27
24	70	4	1.241	998.70	8	18	2.57e − 2	25	6.12e − 2	100	——	——
25	71	8	1.240	999.10	8	19	3.90e − 1	75	6.01e − 2	100	——	——
26	69	9	1.225	1011.7	8	17	8.05e − 1	10	5.86e − 2	50	34	26
27	80	7	1.158	1070.0	9	19	1.23e − 1	75	5.43e − 2	75	38	24
28	81	8	1.177	1052.6	9	20	6.73e − 1	10	3.34e − 2	75	39	25
29	68	8	1.098	1128.9	8	14	1.55e − 1	15	9.17e − 2	75	45	23
30	61	3	1.068	1160.0	6	10	2.72e − 2	25	2.19e − 2	100	7	——
31	100	4	1.029	1204.4	11	21	1.31e − 1	10	7.86e − 2	100	42	21
32	99	3	0.994	1246.9	11	18	7.41e − 1	15	7.83e − 2	100	41	19
33	114	3	0.910	1362.0	12	21	6.49e − 1	10	1.01e − 1	100	——	11

[a]Multiplet number listed in 1996 by Weise et al. [26].
[b]Lower electronic state i and upper electronic state j as defined by Johnston [15].
[c]Multiplet number listed in 1966 by Weise et al. [10].
[d]Multiplet number listed in 1967 by Wilson and Nicolet [5].

Table 3 Summary of the strongest oxygen line multiplets (column definition same as Table 2)

ID no.	Wiese ID	No. of lines	$h\nu$, eV	$\lambda_{CL,mult}$, nm	i	j	f_{ij}	f_{ij} % uncertainty	$\Delta\lambda_{S,0}$, nm	$\Delta\lambda_{S,0}$ % uncertainty	Wiese 66 ID	Wilson 67 ID
1	2	3	9.51	130.35	1	5	5.19e − 2	3	1.64e − 4	50	2	25
2	56	3	1.59	777.55	4	6	1.00e + 0	3	6.30e − 3	50	11	14
3	60	3	1.47	844.88	5	7	1.03e + 0	10	1.28e − 2	50	12	13
4	64	9	1.34	926.64	6	10	9.55e − 1	3	4.44e − 2	50	28	12
5	78	6	1.09	1128.7	7	11	9.85e − 1	3	5.70e − 2	50	29	10

broadening full width at half-height $\Delta\lambda_S$ is also required. For the partially optically thick cases of present interest, the spectrally integrated radiative flux from strong atomic lines depends nearly linearly on $\Delta\lambda_S$, as shown by Johnston [2]. The most comprehensive sources for these values are the theoretical predictions by Griem [11] and Wilson and Nicolet [5]. These studies present values of $\Delta\lambda_S$ for an electron number density N_e of 1×10^{16} particles/cm^3 and at various temperatures. The value of $\Delta\lambda_S$ at this N_e and a temperature of 10,000 K will be labeled here as $\Delta\lambda_{S,0}$ and referred to as the *Stark broadening coefficient*. The value of $\Delta\lambda_S$ at any other temperature and N_e may be approximately related to $\Delta\lambda_{S,0}$ through the following equation [44]:

$$\Delta\lambda_S = \Delta\lambda_{S,0}\left(\frac{T_e}{10,000}\right)^n\left(\frac{N_e}{1\times 10^{16}\text{cm}^{-3}}\right)\ \text{nm} \qquad (1)$$

where the exponent n is chosen to fit the available data. For most nitrogen and oxygen lines, a value of one-third is acceptable [45]. The Stark broadening of each individual line in a multiplet is assumed to be identical, so that only a single $\Delta\lambda_{S,0}$ value is required for each multiplet (which is consistent with the values presented by Griem [11] and Wilson and Nicolet [5]). Even with this assumption, detailed $\Delta\lambda_{S,0}$ values were not available for all lines presently treated. The remaining lines were treated with an approximate correlation, which was chosen using the known $\Delta\lambda_{S,0}$ values as a guide. Applying the curve-fit form suggested by Cowley [46], Arnold et al. [47], and Park [45], the following equation was obtained:

$$\Delta\lambda_{S,0} = \frac{845.0\lambda_{\text{CL}}^2}{(E_{\text{ionize}} - E_u)^{2.623}}\ \text{nm} \qquad (2)$$

with λ_{CL} in nanometers and E_{ionize} and E_u in inverse centimeters. The approximate nature of this equation is sufficient because it is only applied to the lines with no available detailed value, which are nearly all optically thin (with the exception of multiplets 21, 24, 25, and 30 in Table 2) for the conditions of present interest. As a result, the contribution of these lines to the spectrally integrated radiative flux is weakly dependent on the line half-width.

For multiplets with both Griem's [11] and Wilson and Nicolet's [5] $\Delta\lambda_{S,0}$ values available, preference was given to the more recent Griem [11] values, except for the 33 nitrogen and 5 oxygen lines listed in Tables 2 and 3. The values for these important lines are discussed in the following paragraph. For multiplets with no available data, Eq. (2) was applied, as mentioned previously.

For the 33 strong nitrogen multiplets listed in Table 2, the $\Delta\lambda_{S,0}$ values measured by Morris and Garrison [48], Helbig et al. [49], Cullmann and Labuhn [50], Nubbemeyer [51], Goly and Weniger [52], and Sohns and Kock [53] are compared in Fig. 6 with the predictions of Griem [11] and Wilson and Nicolet [5]. In this figure,

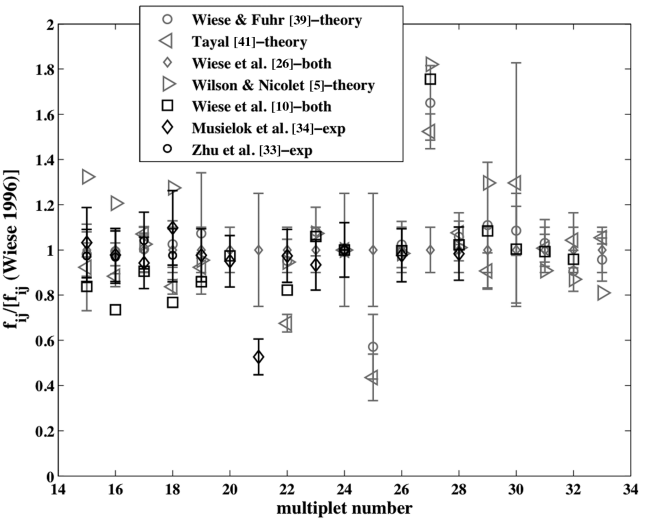

Fig. 5 Summary of predicted and measured multiplet oscillator strengths, normalized by the Wiese et al. [26] values, for multiplets 15–33 listed in Table 2 for nitrogen.

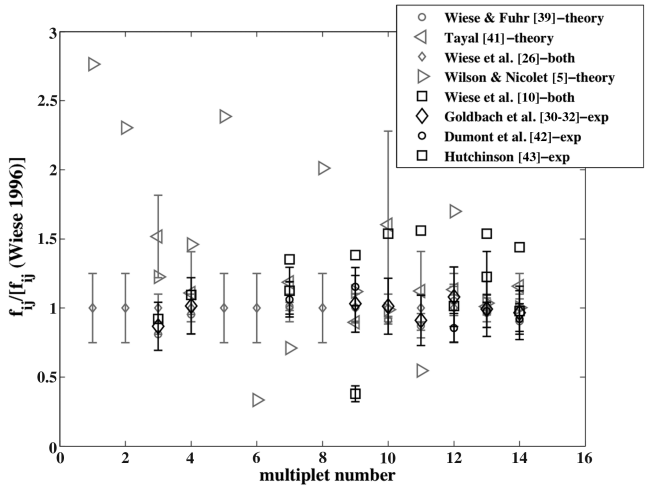

Fig. 4 Summary of predicted and measured multiplet oscillator strengths, normalized by the Wiese et al. [26] values, for the first 14 multiplets listed in Table 2 for nitrogen.

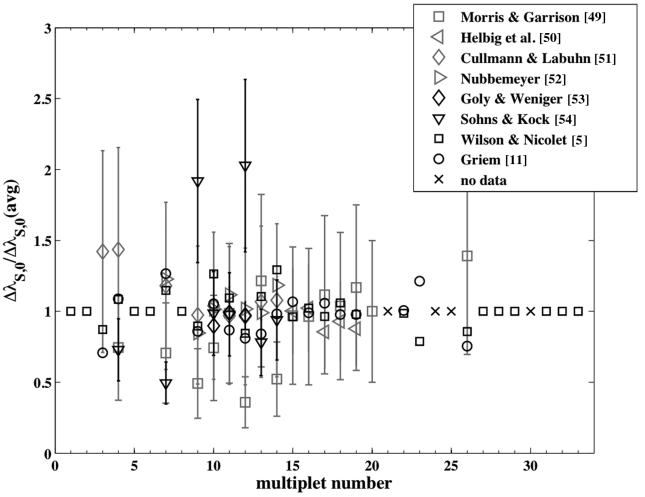

Fig. 6 Comparison of various experimental and theoretical Stark broadening coefficients, normalized by the average, for the 33 nitrogen lines listed in Table 3.

the $\Delta\lambda_{S,0}$ values are normalized by the average of all the presented values for each multiplet. These averaged values are listed in Table 2 and were used throughout the remainder of this study for these strong multiplets. For 11 of these multiplets, the Wilson and Nicolet [5] values were the only available data, whereas for multiplets 21, 24, 25, and 30, there were no available data. For these no-data cases, Eq. (2) is applied.

To accompany the average $\Delta\lambda_{S,0}$ values computed here and applied throughout this study, an uncertainty estimate was made for each multiplet based on the data in Fig. 6. For the multiplets with only the Wilson and Nicolet [5] values available, an uncertainty of 75% was assigned based on the comparison with other multiplets, whereas for the cases with no data, an uncertainty of 100% was conservatively chosen. For the multiplets with various measurements available, it is noted that except for multiplets 7, 9, 12, and 14, the measurement uncertainties overlap the averaged value (meaning that they overlap the value of 1 in the figure) as well as the nominal values from the other measurements and predictions. Considering this, the uncertainty was chosen to capture the nominal values, relative to the average, from all the measurements and theoretical results. The resulting uncertainties are listed in Table 2 for each multiplet.

The remaining details regarding the atomic line data applied in this model are the same as those described by Johnston [15]. The Doppler, resonance, and natural broadening are all treated using the standards expressions. For the line shape, the Voigt profile from Whiting [54] is applied, along with the Voigt width expression from Olivero and Longbothum [55].

For the VUV lines in the case presented in Figs. 2 and 3, the Doppler widths are roughly an order of magnitude larger than the Stark widths, and the resonance broadening contributes only for lines with a ground state lower level. For the IR lines, the Doppler and Stark widths are of nearly equal magnitudes, and the resonance broadening is negligible. The natural width is negligible for both the IR and VUV lines. Note that these relative half-width magnitudes are very dependent on the gas pressure. For example, at the 2-orders-of-magnitude-lower-pressure condition studied by Whiting and Park [56], the Stark broadening was shown to be negligible relative to the Doppler broadening. Note that the lines listed in Tables 2 and 3 are blackbody-limited for this case, which means that the total spectrally integrated flux or intensity is dependent upon the line shapes and widths. As an extension of the present work, Kleb and Johnston [57] assessed the sensitivity of the spectrally integrated radiative flux to the Stark broadening and oscillator strength uncertainties listed in Tables 2 and 3.

III. Atomic Line Numerical Spectrum Modeling

A feature of the present model that allows for a relatively rapid calculation of the radiative spectrum is the nonuniform spacing of the spectral grid. Similar to the RAD/EQUIL and LORAN models, points are arranged in the spectral grid specifically for each line. For a non-optically-thin line, the shape of the emission and absorption coefficient spectrums must be sufficiently modeled for the flux or intensity from that line to be accurately calculated. This requires the use of accurate physical parameters, as discussed in the previous section, as well as the accurate numerical representation of the line shape. For the accurate numerical representation, both the spacing and number of points included in the total spectral grid must be sufficiently chosen for each line.

The distribution of spectral points for each line was achieved using Roberts stretching formula [58]. The main issues in applying this formula are determining the stretching factor, which indirectly sets the distance of the first point away from the centerline, determining the location of the point furthest from the centerline, and determining the number of spectral points used to model each line. For the first of these, it was found that setting the stretching factor to between 1.01 and 1.03, depending on the number of points used to model each line, provided optimal spectral-point spacing for each line. The second of these, determining the point furthest from the centerline, is more complicated because it depends on the optical thickness of the line. Because the goal of the present radiation model is to correctly predict the radiative flux or intensity from a shock layer, the distance from the centerline where 99.9% of the radiative flux is captured is the ideal location for this point. A method for approximately calculating this location for each line was developed by treating the shock layer as a constant-property slab with thickness equal to the actual shock-layer thickness and by setting the temperature and number densities equal to those from the shock layer at the point of maximum electron number density. By applying the Voigt formula proposed by Lui et al. [59] and neglecting the Gaussian contribution (because the line wings are usually dominated by the Lorenztian profile), an analytic formula was derived [15] for the distance away from the centerline where 99.9% of the radiative flux from the representative constant-property slab was captured. This formula results in a nonphysical answer for lines with negligible Lorenztian broadening, for which the Gaussian profile is dominant even in the line wings. For these cases, an analogous formula was derived for the representative constant-property slab by neglecting the Lorenztian contribution (instead of the Gaussian contribution) from the line profile of Liu et al. [59].

The determination of the number of spectral points required for modeling each line was achieved by comparing the radiative flux from layers 1 and 2 of case 2. Figure 7 presents the percent difference in the radiative flux, considering only nitrogen atomic lines, from the $k = 17$ case (where k is the number of points used to model each half of a line). The contributions from the VUV and IR lines are shown separately for the flux resulting from layers 1 and 2. The IR contributions from layers 1 and 2 are indistinguishable (because both the emission and absorption are negligible in layer 2 for these lines), and so they are shown in the figure by a single line. For the VUV lines, layer 2 absorbs roughly 25% of the flux emitted from layer 1, although it is not any more dependent on the line spacing than the other cases. This comparison shows that 9 to 11 spectral points per half-line (meaning 19 to 23 points total for each line, accounting for the center point) are sufficient to model the atomic line radiative flux or intensity through a variable-property layer with an accuracy of at least 2%. A value of 10 points per half-line was applied throughout the remainder of this study. This is actually the minimum number of points used to model each line, because the spectral grid arranged for each line is combined with the grids from all other lines to form a single grid, which results in overlapping grids for closely spaced lines. An alternative discussion regarding the number of points and point spacing for atomic lines was provided recently by Lino da Silva [60], independently of the present work.

The preceding point spacing procedure was applied for non-optically-thin lines, which are determined for each case by comparing the height of the line center resulting from optically thin flux (where the flux is assumed to be equal to 2π multiplied by the emission coefficient) and actual flux, resulting from a constant-property slab with a thickness equal to that of the shock layer. If the

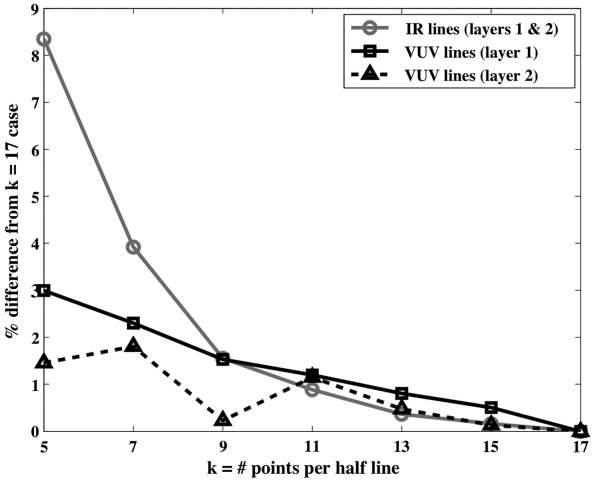

Fig. 7 Influence of the number of spectral points used to model each line, for the double-layer slab case described in the text, on the radiation considering only nitrogen atom lines.

height of the line center for the actual flux is less than 99% of the height of the optically thin line center, then the line is considered to be optically thick, and otherwise it is considered to be optically thin. For the optically thin lines, the detailed treatment of the line shape described in the previous paragraph is not applied. Instead, the line is modeled as a triangle using a total of three points to represent the line. The width of the triangle is assumed to be equal to the Voight width, and the height is chosen so that the frequency-integrated flux from the line is equal to the optically thin flux from the line. This procedure reduces the computational cost for the line calculation with a negligible loss in accuracy. Most of the thousands of OP lines described previously are optically thin for conditions of present interest, making this procedure particularly useful.

IV. Atomic Bound–Free and Atomic Free–Free Radiation

Bound-free radiation is the result of a bound electron being excited to an energy level above the ionization energy, which results in the bound electron becoming a free electron (Zel'dovich and Raizer [61], pp. 248–276). The absorption coefficient resulting from this process is written as

$$\kappa_{\nu,i}^{\mathrm{bf}} = \sigma_{\nu,i}^{\mathrm{bf}} N_i \ \mathrm{cm}^{-1} \tag{3}$$

where $\sigma_{\nu,i}^{\mathrm{bf}}$ is the absorption cross section of level i and N_i is the number density of this level. The corresponding emission coefficient may be derived by assuming that it is proportional to the ion and electron number densities and a function $\Phi_{\nu,i}$ that is independent of the atomic state populations and the ion or electron number densities:

$$j_{\nu,i}^{\mathrm{bf}} = N_+ N_e \Phi_{\nu,i} \ \mathrm{erg}/(\mathrm{cm}^3 \cdot \mathrm{sr}) \tag{4}$$

The function $\Phi_{\nu,i}$ can be related to $\sigma_{\nu,i}^{\mathrm{bf}}$ by applying Kirchoff's law, which may be written as

$$j_{\nu,i,\mathrm{EQ}}^{\mathrm{bf}} = \frac{2h\nu^3}{c^2} \kappa_{\nu,i,\mathrm{EQ}} \exp\left(-\frac{h\nu}{hT_e}\right) \ \mathrm{erg}/(\mathrm{cm}^3 \cdot \mathrm{sr}) \tag{5}$$

where the subscript EQ indicates that the electron, ion, and atomic state number densities used in the emission and absorption coefficients satisfy the Saha–Boltzmann equation:

$$\left(\frac{N_+ N_e}{N_i}\right)_{\mathrm{EQ}} = \frac{2Q_+}{g_i} \left(\frac{2\pi m k T_e}{h^2}\right)^{3/2} \exp \frac{hc(E_i - E_{\mathrm{ionize}})}{kT_e} \tag{6}$$

The requirement that the Saha–Boltzmann equation must be satisfied for Kirchoff's law to be valid implies that both the atomic states are populated in a Boltzmann distribution and that chemical equilibrium exists among the atoms, ions, and electrons. This is in contrast to bound–bound radiation, where only a Boltzmann distribution of the atomic states is required for Kirchoff's law to be valid. Combining Eqs. (3–6) and solving for $\Phi_{\nu,i}$ results in the following:

$$\Phi_{\nu,i} = \frac{2h\nu^3}{c^2} \frac{g_i}{2Q_+} \left(\frac{h^2}{2\pi m k T_e}\right)^{3/2} \times \sigma_{\nu,i}^{\mathrm{bf}} \exp\left[\frac{hc(E_{\mathrm{ionize}} - E_i) - h\nu}{kT_e}\right] \mathrm{erg} \cdot \mathrm{cm}^3 \tag{7}$$

Note that, as was assumed previously, this function is independent of the electron, ion, and excited state number densities. This fact makes Eq. (7) valid regardless of whether there is chemical equilibrium or a Boltzmann distribution of electronic states. Combining Eqs. (4) and (7), the bound–free emission coefficient from a single level i becomes

$$j_{\nu,i}^{\mathrm{bf}} = N_+ N_e \frac{2h\nu^3}{c^2} \frac{g_i}{2Q_+} \left(\frac{h^2}{2\pi m k T_e}\right)^{3/2} \times \sigma_{\nu,i}^{\mathrm{bf}} \exp\left[\frac{hc(E_{\mathrm{ionize}} - E_i) - h\nu}{kT_e}\right] \mathrm{erg}/(\mathrm{cm}^3 \cdot \mathrm{sr}) \tag{8}$$

The bound–free absorption cross sections $\sigma_{\nu,i}^{\mathrm{bf}}$ required for Eqs. (3) and (8) were obtained from the Opacity Project's online database of photoionization cross sections, called the TOPbase [14]. This database provides spectrally resolved cross sections for all the levels of all the atoms and ions of present interest. In fact, the spectral resolution is so great and requires so many frequency points (over 12,000 for nitrogen) that a method of approximating the data using fewer frequency points is required for the practical computation of radiative heat flux through a shock layer. In the present study, two different forms of approximation for modeling the cross-sectional frequency dependence are applied. The cross sections for the first three levels of oxygen and nitrogen are represented with a step model consisting of enough steps to sufficiently model many of the discrete linelike features of the bound–free spectrum. The step models created for nitrogen and oxygen are listed in Appendix B of [15]. The cross sections for the remaining levels are approximated by the following function:

$$\sigma_{\nu,i}^{\mathrm{bf}} = \sigma_{\mathrm{thresh},i}^{\mathrm{bf}} \left(\frac{h\nu_{\mathrm{thresh},i}}{h\nu}\right)^{\theta_i} \ \mathrm{cm}^2 \tag{9}$$

where the parameters $\sigma_{\mathrm{thresh},i}^{\mathrm{bf}}$, $h\nu_{\mathrm{thresh},i}$, and θ_i are chosen to give the best fit through the TOPbase data, and are listed in Appendix B of [15]. This approximate treatment of the TOPbase cross sections produces flux and intensity values that are nearly indistinguishable from the results of the exact cross sections [15]. The TOPbase cross sections have been compared with the less detailed values presented by Hofsaess [62]. The total flux values predicted by the two models agree within 5% for the conditions of present interest.

The finite number of levels treated for nitrogen and oxygen in the present model result in the neglecting of the bound–free radiation from the higher, untreated, levels. The bound–free radiation from these levels, which are near the ionization limit, is similar to atomic free–free radiation. It was found convenient and sufficient to treat both the bound–free radiation from the untreated atomic levels and the free–free radiation together using the Biberman continuum described in [63], which is written for this purpose as

$$\kappa_{\nu}^{\mathrm{Biberman}} = N_+ N_e \frac{4}{3} \left(\frac{2\pi}{3mkT_e}\right)^{1/2} \frac{Z^2 e^6}{hcm\nu^3} \xi(\nu) \exp\left(\frac{h\bar{\nu}}{kT_e}\right) \ \mathrm{cm}^{-1} \tag{10}$$

where

$$\bar{\nu} = \nu \quad \text{for } \nu < \nu_{\mathrm{thresh}}, \qquad \bar{\nu} = \nu_{\mathrm{thresh}} \quad \text{for } \nu \geq \nu_{\mathrm{thresh}} \tag{11}$$

and the threshold frequency ν_{thresh} is the photoionization edge location of the highest treated level. This is roughly 0.2 eV for both nitrogen and oxygen in the present model. The $\xi(\nu)$ factor is obtained from Biberman and Norman [64]. Note that Eqs. (10) and (11) are written in terms of N_+ and N_e, instead of the usual N_a, to remove the restriction of chemical equilibrium. The corresponding emission coefficient is written as

$$j_{\nu}^{\mathrm{Biberman}} = N_+ N_e \frac{8}{3} \left(\frac{2\pi}{3mkT_e}\right)^{1/2} \times \frac{Z^2 e^6}{c^3 m} \xi(\nu) \exp\left(\frac{h\bar{\nu}}{kT_e} - \frac{h\nu}{kT_e}\right) \mathrm{erg}/(\mathrm{cm}^3 \cdot \mathrm{sr}) \tag{12}$$

In summary, Eqs. (3) and (8) are applied for the bound–free radiation using the curve-fitted TOPbase cross sections for 35 and 32 levels of oxygen and nitrogen, respectively, and Eqs. (10) and (12) are applied to treat the free–free radiation as well as the bound–free radiation from the higher levels of oxygen and nitrogen.

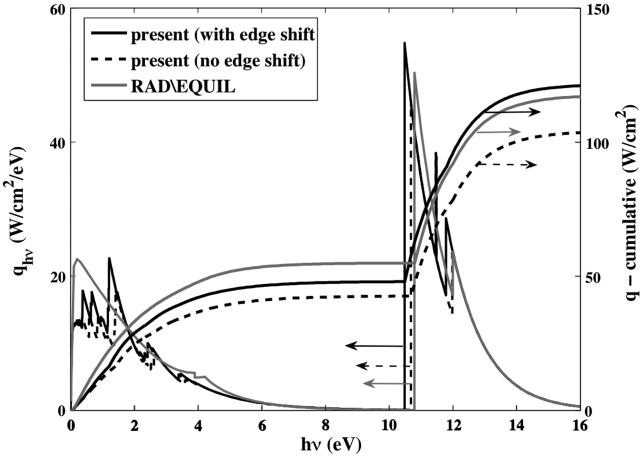

Fig. 8 Nitrogen bound–free and free–free radiative-flux comparison for case 1.

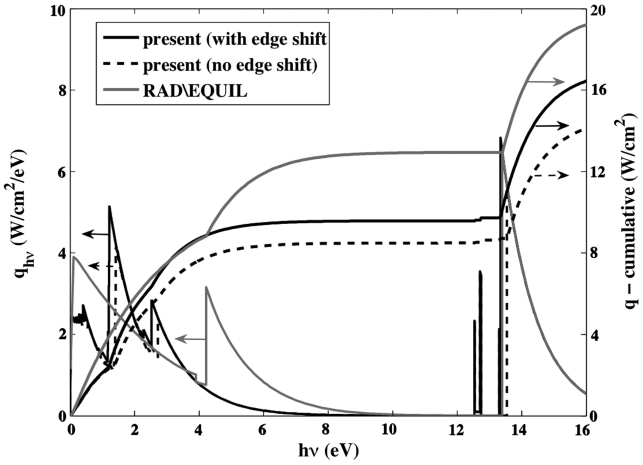

Fig. 9 Oxygen bound–free and free–free radiative-flux comparison for case 1.

Armstrong [37] described an alteration to the bound–free spectrum required to accommodate the atomic line transitions with upper levels very close to the ionization limit. These upper levels include those with a principal quantum number of 8 or above. Although these lines are not included in the NIST database by Wiese et al. [26], many of them are included in the OP database [35], as discussed previously in Sec. II. The alteration to the bound–free spectrum suggested by Armstrong [37] requires the shifting of the photoionization edges by the following frequency increment:

$$\Delta h\nu = -1.79 \times 10^{-5} \frac{N_e^{2/7}}{T_e^{1/7}} \text{ eV} \tag{13}$$

where N_e is the electron number density in particles per cubic centimeter and T_e is in Kelvin. This negative frequency shift is applied to the TOPbase cross sections by extrapolating them to the lower frequency limit. For the bound–free contribution from Eqs. (10) and (12), this alteration is accounted for by multiplying these equations by $\exp(\Delta h\nu/kT_e)$, as suggested by Wilson and Nicolet [5]. The influence of this edge shift for case 1 is shown in Figs. 8 and 9 for nitrogen and oxygen, respectively. The value of $\Delta h\nu$ for this case is -0.19 eV. For nitrogen, it is seen that the inclusion of the edge-shift results in a 16 W/cm^2 increase in the integrated flux, with a roughly equal increase above and below 6 eV. This increase is compared with the 30 W/cm^2 increase due to the OP lines shown in Fig. 3, which represents a more detailed treatment of this mechanism. Because the OP line contribution is greater than the edge-shift contribution, it is concluded that the OP lines sufficiently account for the atomic lines with upper levels near the ionization limit. Therefore, the results presented in the remainder of this study will not include the photoionization edge shift.

V. Negative-Ion Continuum

Numerous experimental studies [65–73] of the radiation from high-temperature air have noted measured continuum-radiation values larger than those predicted by the combination of molecular-band, atomic bound–free, and atomic free–free mechanisms. This phenomenon has been attributed to the negative-ion photodetachment continuum by many researchers, although it has also been suggested to result from the overlapping of lines with upper states near the ionization limit [74] or overlapping Holtsmark line wings [75]. Nevertheless, the negative-continuum contribution from both N^- and O^- are treated in the present model to ensure conservatism in the radiative-flux prediction. The absorption coefficient due to the negative continuum is written as

$$\kappa_{\nu,i-}^{-} = \sigma_\nu^- \left\{ \frac{N_a N_e g_{i-} h^3}{2(2\pi m k T_e)^{3/2} Q_a} \exp\left[\frac{hc}{kT_e} (E_{i-} - E_i) \right] \right\} \text{ cm}^{-1} \tag{14}$$

where the term in brackets represents the number density of the electronic level of the radiating negative ion, calculated using the Saha relationship. The process modeled by Eq. (14) is written schematically as

$$A^-(i-) + h\nu \rightarrow A(i) + e^- \tag{15}$$

where A and A^- represent the neutral atom and negative ion, respectively. The most recent review of the negative-ion contribution in air has been made by Soon and Kunc [76] and Chauveau et al. [77]. The theoretically derived cross sections suggested by Soon and Kunc [76] for the $N^-(^3P)$ and $N^-(^1D)$ levels and the $O^-(^2P)$ cross section suggested by Chauveau et al. [77] were applied in the present model and are listed in Table 4, which also lists the energies and degeneracies required for Eq. (14). These cross sections are on the low end of proposed values [73] for N^-, which are suggested in some experimental studies to be up to an order of magnitude greater [69,71].

The negative-ion emission, which is calculated from κ_ν using Kirchoff's law (even for nonequilibrium conditions) is optically thin in the 1–8-eV range where its contribution is most significant. The last column in Table 4 lists the radiative-flux contribution from each negative-ion transition for case 1. The total value of 22.8 W/cm^2 is less than the 59 W/cm^2 predicted by the optional negative-continuum treatment in the RAD/EQUIL code (which has not been applied in most published results [19]) based on the data of Morris et al. [67].

Table 4 Parameters used for calculating the negative-ion spectrum

$A^-(i-)$	$A(i)$	g_{i-}	E_{i-}, eV	E_i, eV	σ_ν^-, cm^2	Flux, W/cm^2
$N^-(^3P)$	$N(^4S)$	9	0.1	0.0	5e − 18 ($0.7 < h\nu < 2.43$ eV) 1e − 17 ($2.43 < h\nu < 13.0$ eV)	20.3
$N^-(^1D)$	$N(^2D)$	5	1.44	2.38	5e − 18 ($1.32 < h\nu < 2.43$ eV) 1e − 17 ($2.43 < h\nu < 13.0$ eV)	2.2
$O^-(^2P)$	$O(^3P)$	5	1.49	0.0	1e − 17 ($1.49 < h\nu < 13.0$ eV)	0.3

VI. Modeling of Molecular-Band Systems

The radiation resulting from molecular species in equilibrium air at conditions relevant to lunar-return shock layers is usually no more than 7% of the total radiative flux. At *nonequilibrium* conditions, this contribution can increase slightly, depending on the shock-layer thickness and nonequilibrium region, but conditions in which this is significant usually occur away from peak-heating conditions, where the total radiative flux is relatively small. Because molecular-band systems do not contribute significantly, it was desired to model them using a computationally inexpensive technique that provides reasonably accurate results. The SRB method developed by Patch et al. [78] was chosen for this purpose. This method was extended by Chambers [10] to higher-order accuracy and multitemperature conditions. From Chambers, the equations for the absorption and emission coefficients for a single molecular-band system are written as follows

$$\kappa_\nu^{\text{band}} = N_{e''}\frac{\pi e^2}{mc^2}\sum_{V''}\sum_{V'}\frac{1}{|B_{V'}-B_{V''}|}\frac{f_{V''V'}}{Q_J Q_V} \times \exp\left(-\frac{hc}{kT_v}E_{V''}\right)\exp\left(-\frac{hc}{kT_r}E_{J''}\right)\ \text{cm}^{-1} \tag{16}$$

$$j_\nu^{\text{band}} = N_{e'}\frac{2h\pi e^2}{mc^4}\frac{g_{e''}}{g_{e'}}\sum_{V''}\sum_{V'}\frac{\nu^3}{|B_{V'}-B_{V''}|}\frac{f_{V''V'}}{Q_J Q_V} \times \exp\left(-\frac{hc}{kT_v}E_{V'}\right)\exp\left(-\frac{hc}{kT_r}E_{J'}\right)\ \text{erg}/(\text{cm}^3\cdot\text{sr}) \tag{17}$$

The various terms in these equations are defined in the Nomenclature, except for the rotational energy, which is approximated as follows:

$$E_J = \frac{B_e}{B_{e'}-B_{e''}}\ \frac{(\nu-\nu_{V'V''})}{c}\ \text{cm}^{-1} \tag{18}$$

The simplicity of applying the SRB approach is seen by writing the absorption coefficient as

$$\frac{\kappa_\nu^{\text{band}}}{N_{e''}} = \phi(\nu)\sum_{n=1}^{NN}P_{V'V'',n} \qquad \nu_{V'V'',n-1}\le\nu\le\nu_{V'V'',n} \tag{19}$$

where

$$P_{V'V'',n} = \frac{\pi e^2}{mc^2}\frac{1}{|B_{V'}-B_{V''}|} \times \frac{f_{V''V'}}{Q_J Q_V}\exp\left(-\frac{hc}{kT_v}E_{V''}\right)\exp\left(\frac{h}{kT_r}\frac{B_e}{B_{e'}-B_{e''}}\nu_{V'V''}\right) \tag{20}$$

and

$$\phi(\nu) = \exp\left(-\frac{h}{kT_r}\nu\frac{B_{e''}}{B_{e'}-B_{e''}}\right) \tag{21}$$

The limiting frequencies for Eq. (19) may be calculated for each V'-V'' transition as

$$\nu_{V'V'',n} = c\left[E_{e'}-E_{e''}+E_{V'}-E_{V''}-\frac{1}{4}\frac{(B_{V'}+B_{V''})^2}{(B_{V'}-B_{V''})}\right] \tag{22}$$

The last term in this equation, suggested by Golden [79], improves the agreement between this method and the line-by-line approach. The subscript n on $P_{V'V''}$ and $\nu_{V'V''}$ is assigned by sorting the $\nu_{V'V''}$ values in ascending or descending order, depending on the sign of $B_{e'}$-$B_{e''}$ for the band system (ascending if positive, descending if negative).

The accuracy of the SRB method may be gauged relative to the results of the detailed line-by-line (LBL) method, which is described in detail in Appendix D of [15] for the simple case of a $^2\Sigma$–$^2\Sigma$ transition. This case is of interest for the CN violet molecular band, which was studied by Johnston et al. [80], among others, for Titan entry. By comparing the SRB and LBL results, Johnston showed that the SRB method was insufficient (for the specific case of Huygens entry into Titan) because the spectrum was partially optically thick. As a result, the SRB method overpredicted the integrated flux by up to 40% relative to the LBL method. Fortunately, the most significantly emitting-band system for air (at conditions of present interest) will be shown in the next section to be the N_2^+ first negative band system, which is also a $^2\Sigma$–$^2\Sigma$ transition. Thus, the LBL method described in Appendix D of [12] may be applied to this band system and compared with the SRB results for conditions typical of a lunar-return shock layer. For a 4-cm constant-property slab of equilibrium air at 1 atm and 10,000 K, Fig. 10 compares a limited region of the radiative-flux spectrum predicted by the SRB and LBL methods. Although the two spectrums appear to be very different, they actually predict spectrally integrated flux values that agree within 4% (resulting from integration over the entire spectrum, not just the range shown in the figure). The reason for this good agreement is that the spectrum is optically thin, which is indicated in the figure by the Planck function B_{h_ν} being significantly larger than any of the peaks in either the SRB or LBL spectrum (note that the B_{h_ν} curve shown was divided by 30 so that it is in the range of the figure's vertical axis). The SRB method is guaranteed, as a result of its derivation, to accurately reproduce the optically thin flux. Thus, the fact that the strongest molecular-band emitter in air is optically thin for the conditions of present interest indicates that the SRB method is sufficient for treating the *emitting* band systems. For the strongly *absorbing* band systems in the VUV, this conclusion is not applicable. The influence of the absorbing-band systems on the radiative flux, along with the validity of the SRB model for these bands, will be discussed in Sec. VII.

The 15 molecular-band systems presently treated for air are listed in Table 5. The data required to implement these band systems were taken mostly from Laux [81], although for the VUV systems, various other sources were used [82–85]. The oscillator strengths for the Birge–Hopfield I and II systems were not available for many of the vibrational transitions. These values were estimated using the Franck–Condon factors from Generosa [85] and the available oscillator strengths summarized by Chauveau et al. in [84]. The uncertainty of these approximate values is estimated to be a factor of 2. The total molecular-band flux for case 1 is 18.2 W/cm^2, which is less than 5% of the total radiative flux for this case. The flux contribution from each band system is listed in the last column of Table 5.

A comparison of the molecular-band radiative flux predicted by the present model and RAD/EQUIL, accounting for only molecular-band emission and absorption, is shown in Fig. 11 for case 1. The RAD/EQUIL model is based on spectrally smoothed curve fits. It

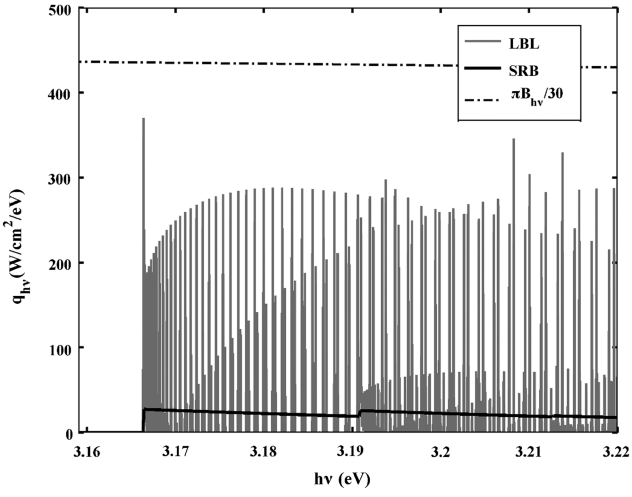

Fig. 10 Comparison of the N_2^+ 1$^-$ flux predicted by the LBL and SRB methods for a 4-cm constant-property slab at 1 atm and 10,000 K.

Table 5 Molecular band systems treated for air in the present model

Molecule	Transition	Name	Spectral range, eV	Reference	Flux,[a] W/cm^2
N_2	$B^3\Pi_g$–$A^3\Sigma_u^+$	1^+ (first positive)	0.2–2.5	[81]	0.26
N_2	$C^3\Pi_u$–$B^3\Pi_g$	2^+ (second positive)	2.7–4.7	[81]	0.94
N_2	$c_4'\Sigma_u^+$–$X^1\Sigma_g^+$	Carroll–Yoshino	11.5–14.0	[82–84]	0.18
N_2	$c_3'\Pi_u$–$X^1\Sigma_g^+$	Worley–Jenkins	11.5–14.0	[82–84]	0.16
N_2	$b^1\Pi_u$–$X^1\Sigma_g^+$	Birge–Hopfield I	7.0–13.1	[83–85]	1.14
N_2	$b'^1\Sigma_u^+$–$X^1\Sigma_g^+$	Birge–Hopfield II	7.6–14.0	[82–84]	0.91
N_2	$o_3{}^1\Pi_u$–$X^1\Sigma_g^+$	Worley	10.4–14.0	[82–84]	0.27
N_2^+	$B^2\Sigma_u^+$–$X^2\Sigma_g^+$	1^- (first negative)	1.2–4.6	[81]	11.77
NO	$B^2\Pi_r$–$X^2\Pi_r$	β (beta)	2.1–6.9	[81]	0.26
NO	$A^2\Sigma^+$–$X^2\Pi_r$	γ (gamma)	3.2–7.5	[81]	0.39
NO	$C^2\Pi_r$–$X^2\Pi_r$	δ (delta)	3.7–7.6	[81]	0.73
NO	$D^2\Sigma^+$–$X^2\Pi_r$	ε (epsilon)	3.4–8.0	[81]	0.69
NO	$B'^2\Delta$–$X^2\Pi_r$	β' (beta-prime)	3.9–8.4	[81]	0.21
NO	$E^2\Sigma^+$–$X^2\Pi_r$	γ' (gamma-prime)	4.6–8.9	[81]	0.22
O_2	$B^3\Sigma_u^-$–$X^3\Sigma_g^+$	Schumann–Runge	2.6–7.0	[81]	0.08

[a]Radiative-flux contribution in W/cm^2 for case 1 due to the emission of the specified band system and absorption from all mechanisms.

accounts for all of the presently treated band systems, except for the N_2 Worley–Jenkins, Worley, and Carroll–Yoshino systems. The lower prediction from the present model in the 2–4-eV range is due mostly to the N_2^+ 1^- band system, for which the flux is roughly half of the RAD/EQUIL prediction. Because the absorption from atomic lines and continuum is not included in this comparison, the contribution from the VUV band systems shown in Fig. 11 is larger than that listed in Table 5.

VII. Results of the Air-Radiation Model in Equilibrium

To summarize the contributions from the various radiative mechanisms described in the previous sections, Fig. 12 presents the contribution to the radiative flux from each mechanism for case 1 (the spectrum is plotted with the left axis, which is a log scale, and the cumulative curves are plotted with the right axis, which is linear). The flux components shown are calculated by applying the emission coefficient of the specified mechanism, along with the total-absorption coefficient (from all mechanisms and species), in the radiation transport equation. This is done so that the addition of the various components results in the total flux, which is 373 W/cm^2 (233 W/cm^2 below 6 eV) for this case. The dominance of atomic nitrogen radiation is apparent in this figure, as is the relatively small molecular-band contribution.

To complete the comparisons between the present model and the RAD/EQUIL code, Fig. 13 presents the total flux spectrum and cumulative flux for case 1 (comparisons between the individual radiative mechanisms were presented in the previous sections). The RAD/EQUIL results presented here are results of the actual RAD/EQUIL code, whereas the results of the previous sections were obtained by applying RAD/EQUIL's atomic line, continuum, and molecular-band data using the present code. This explains the steplike nature of the RAD/EQUIL continuum above 10 eV in Fig. 13, which is a result of RAD/EQUIL's "line grouping" approximation (that assumes a constant continuum value and Planck function over a specified spectral range). Figure 13 shows that the flux predicted by the present model below 6 eV is 34 W/cm^2 larger than the RAD/EQUIL prediction. Figures 3, 8, 9, and 11 indicate that this is a result of the present model's roughly 50 W/cm^2 larger contribution from the atomic lines (below 6 eV) minus the roughly 22 W/cm^2 smaller contribution from the atomic continuum and roughly 15 W/cm^2 smaller contribution from the molecular-band systems. In addition, the present model includes the 22.8 W/cm^2 contribution from the negative continuum (Table 4), whereas the RAD/EQUIL result does not include this mechanism. This cancellation of differences between RAD/EQUIL and the present model explains how the individual components presented in the previous sections can each disagree by no less than 20%, whereas the total integrated flux values presented in Fig. 13 agree by better than 10%.

A comparison of the flux resulting from layer 2 of case 2 is shown in Fig. 14. As mentioned previously, layer 2 approximates the boundary layer present near the body of a shock-layer flowfield, which is expected to absorb some of the flux resulting from the larger inviscid shock-layer region represented by the 15-cm slab. The flux below 6 eV is essentially unaltered from the results of Fig. 13 (note that case 1 is the same as layer 1 of case 2) because of the weak absorption in this spectral range. Above 6 eV, the absorption is

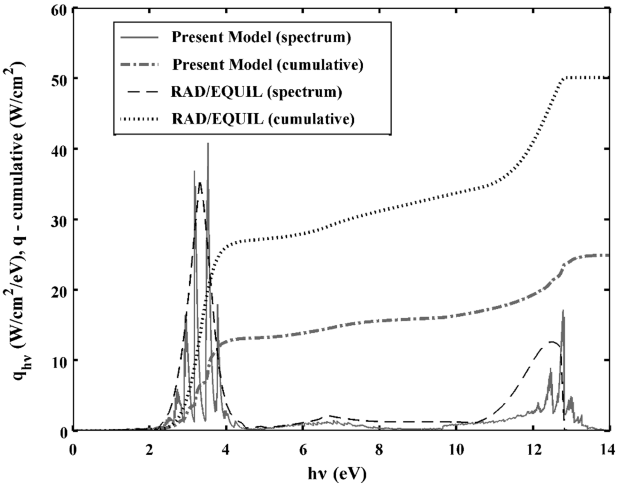

Fig. 11 Radiative flux resulting from only molecular-band emission and absorption predicted by the present model and RAD/EQUIL.

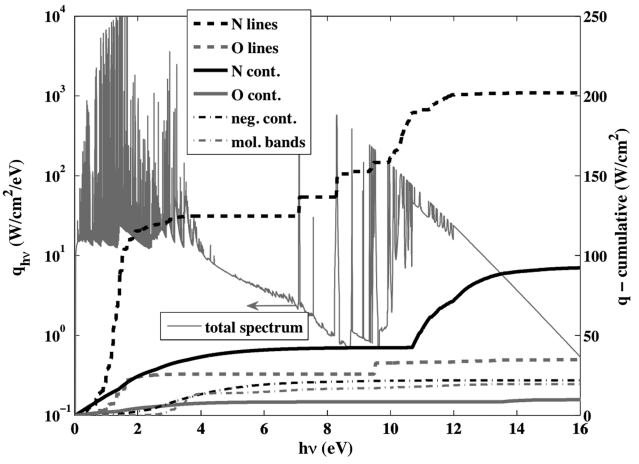

Fig. 12 Contributions from the various radiative mechanisms to the radiative flux of a 15-cm slab of equilibrium air at 10,000 K and 0.5 atm.

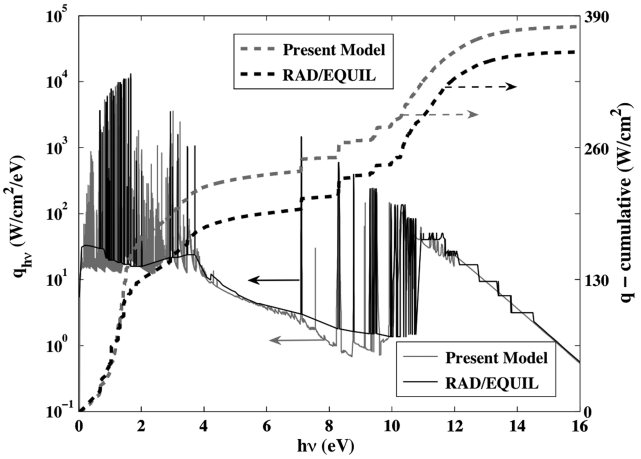

Fig. 13 Radiative flux for case 1 (or layer 1 of case 2) predicted by the present model and RAD/EQUIL (solid lines are the flux spectrums and are plotted using the left axis, and dashed lines are the cumulative fluxes and are plotted using the right axis).

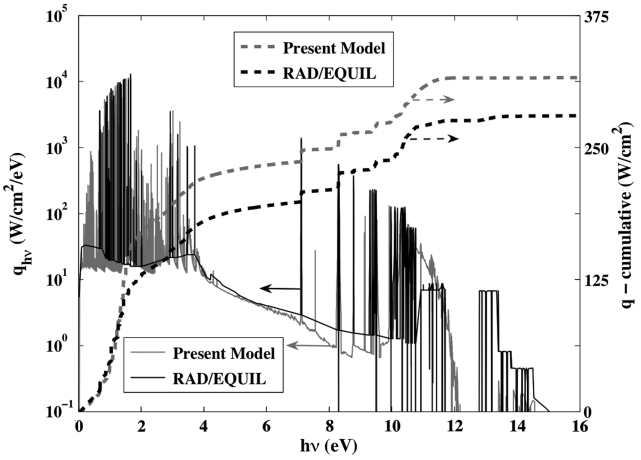

Fig. 14 Radiative flux for layer 2 of case 2 predicted by the present model and RAD/EQUIL (same solid- and dashed-line definitions as Fig. 13).

significant, with the present model being reduced by 63 W/cm^2, whereas the RAD/EQUIL result is reduced by 75 W/cm^2. This slight difference in absorption is a result of RAD/EQUIL's increased absorption from the Birge–Hopfield I and II band systems, which accounts for roughly half of the VUV absorption. Neglecting the VUV band systems decreases the 63 W/cm^2 of absorption to 33 W/cm^2 for the present model, and decreases the 75 W/cm^2 of absorption to 31 W/cm^2 for RAD/EQUIL. Note that this absorbed flux by the VUV band systems is almost twice as large as the emitted flux from all band systems shown in Table 5.

As presented in Sec. VI, the SRB treatment of the strongly *emitting* molecular-bands systems, which are located in the 2–4-eV range, is accurate because they are optically thin for the conditions of present interest. However, the validity of the SRB treatment for strongly *absorbing* band systems, which are located in the 10–12-eV range, was not proven. As was just discussed, the influence of molecular-band absorption in the VUV is significant. To validate the SRB treatment of absorbing-band systems, Fig. 15 compares the VUV flux (between 10.5 and 13 eV) from layer 2 of case 2 obtained by either ignoring the VUV band systems, treating them with an LBL model, or treating them with the present SRB model (note that the cumulative flux starts at 10.5 eV). The same oscillator strengths and energy levels as presented in Sec. VI for the SRB model are used also for the LBL model. It should be emphasized that the LBL model requires many orders of magnitude greater computational time than the SRB model (and in fact the entire present radiation calculation)

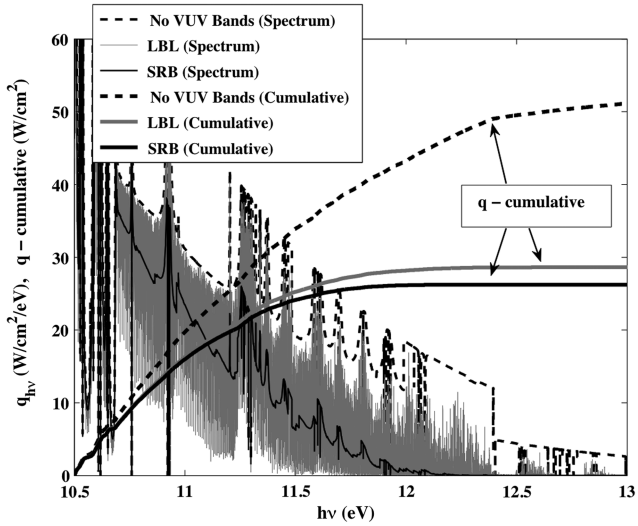

Fig. 15 VUV radiative flux from layer 2 of case 2 obtained by either ignoring the VUV bands, treating them with an LBL model, or treating them with an SRB model.

[80]. By comparing the SRB and LBL cumulative results with the no-VUV-band result, it is shown that the molecular-band absorption predicted by the SRB and LBL models result in a 25.2 and 22.8 W/cm^2 reduction in the flux, respectively. This good agreement is encouraging considering the differences in the spectrums shown in Fig. 15. Although the SRB result does not capture the peaks and valleys of the LBL model's rotational lines, it does nearly capture the average of these extremes, which allows it to closely match the total cumulative flux of the LBL model. This result for the treatment of absorbing-band systems with the SRB approach provides further confidence in its application for lunar-return conditions.

The comparison between the present model and RAD/EQUIL is presented in Fig. 16 for case 3, which consists of a 15-cm constant-property slab at 0.5 atm and 8000 K, instead of 10,000 K. The lower temperature causes the molecular-band systems to be the dominant contributor. For this case, the RAD/EQUIL predicts a total molecular-band contribution of 29 W/cm^2 and a total line contribution of 8 W/cm^2, whereas the present model predicts a total molecular-band contribution of 17 W/cm^2 and a total line contribution of 11 W/cm^2 (along with an additional 4 W/cm^2 from the negative continuum). The larger molecular-band prediction from RAD/EQUIL causes its total flux to be larger than that from the present model, unlike the 10,000 K case, for which the atomic line contribution was dominant and the present model predicted a larger flux.

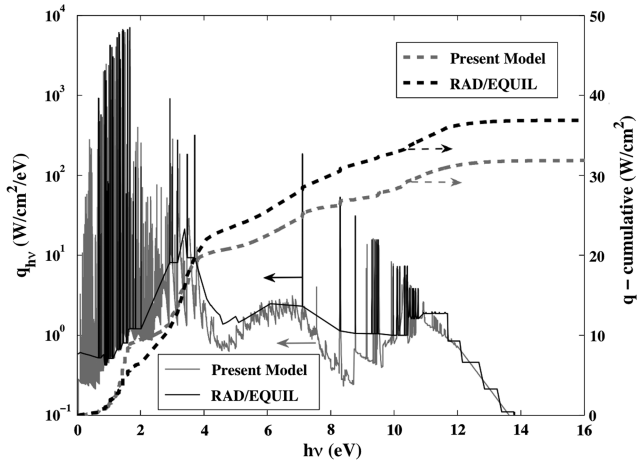

Fig. 16 Radiative flux for case 3 predicted by the present model and RAD/EQUIL (same solid- and dashed-line definitions as Fig. 13).

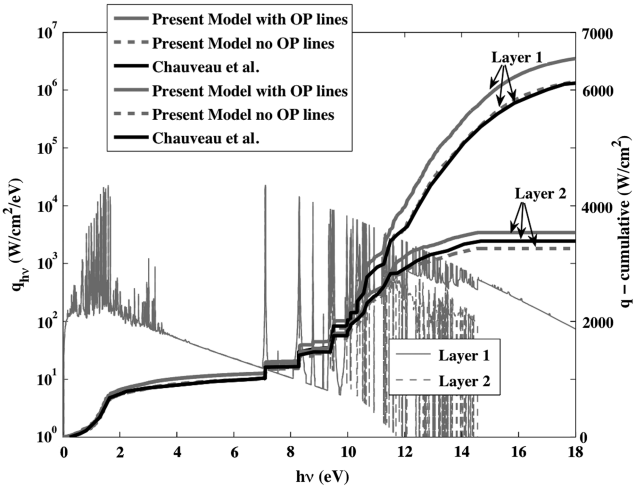

Fig. 17 Radiative flux for layers 1 and 2 of case 4 predicted by the present model and by Chauveau et al. [77].

As a final assessment of the present model, the double-layer example presented by Chauvaeu et al. [77] and defined as case 4 in Table 1 is considered. Each layer consists of equilibrium air at 1 atm, with the first layer having a thickness of 0.8 cm and a temperature of 15,000 K and the second layer having a thickness of 0.4 cm and a temperature of 8000 K. Figure 17 presents the flux spectrum and cumulative flux predicted by the present model at the edge of each layer. Also shown are the cumulative-flux values from the present model neglecting the OP lines and the cumulative flux predicted by Chauveau et al., which do not include the OP lines. For layer 1, the difference between the results of Chauveau et al. and the present result without OP lines is nearly indistinguishable. For layer 2, the agreement is also good, with both results showing significant VUV absorption. The results of Chauveau et al. include the LBL treatment of molecular-band systems, instead of the approximate SRB treatment applied in the present model. The present model predicts that roughly 500 W/cm^2 of the reduction between layers 1 and 2 is due to VUV molecular-band systems. Therefore, the good agreement between the present model and the Chauveau et al. result provides further validation for the application of the SRB model for VUV absorption.

VIII. Conclusions

New models for atomic lines, bound–free photoionization, negative-ion continuum, and molecular bands were developed. The atomic line model was based on the most recent experimental and theoretical oscillator strengths and Stark broadening half-widths. The uncertainty of these parameters was quantified by gathering and comparing available data, and it was found that the uncertainties are larger than those listed by NIST. All lines listed in both the NIST and Opacity Project databases were included in the present model. The addition of the Opacity Project lines, for lines not accounted for in the NIST database, was shown to increase the atomic line flux by up to 15%. For the conditions of present interest, it was found that this new atomic line model predicts up to a 50% larger atomic line flux in the spectral region below 6 eV than previous models. A new atomic photoionization model was applied based on the data compiled in the TOPbase. This new model contains significant spectral detail, which was simplified using a combination of curve fits and step models. The application of the photoionization edge shift was studied and shown to model many of the atomic lines listed in the Opacity Project with an upper electronic state principal quantum number greater than 8. Modeling of the negative-ion continuum was reviewed and its contribution was found to be roughly 5–8% of the total flux. The molecular-band systems were treated using the SRB method. For the presently studied lunar-return conditions, the accuracy of the SRB model for both strongly emitting and strongly absorbing band systems was shown to be excellent relative to the more computationally intensive line-by-line method. Molecular-band absorption in the VUV was shown to absorb up to 10% of the total flux. The comparisons of this new radiation model with the RAD/EQUIL code indicated differences of *no less* than 20% for the atomic line, atomic bound–free, and molecular-band contributions to the radiative flux. Because these differences were both positive and negative, and therefore cancelled each other, the difference in the total radiative flux was only 10–15% for the cases studied. Considering both the increase in the atomic line model and the inclusion of the negative-ion continuum, the total radiative flux predicted by the present model is as much as 20% greater than previous models [4,9,15] for conditions relative to a peak-heating lunar-return shock layer.

References

[1] Grinstead, J., Wilder, M., Olejniczak, J., Bogdanoff, D., Allen, G., and Danf, K., "Shock-Heated Air Radiation Measurements at Lunar Return Conditions," AIAA Paper 2008-1244, 2008.

[2] Johnston, C. O., "A Comparison of EAST Shock-Tube Radiation Measurements with a New Air Radiation Model," AIAA Paper 2008-1245, 2008.

[3] Bose, D., McCorkle, E., Thompson, C., Bogdanoff, D., Prabhu, D., Allen, G., and Grinstead, J., "Analysis and Model Validation of Shock Layer Radiation in Air," AIAA Paper 2008-1246, 1008.

[4] Nicolet, W. E., "Advanced Methods for Calculating Radiation Transport in Ablation-Product Contaminated Boundary Layers," NASA CR-1656, 1970.

[5] Wilson, K. H., and Nicolet, W. E., "Spectral Absorption Coefficients of Carbon, Nitrogen, and Oxygen Atoms," *Journal of Quantitative Spectroscopy and Radiative Transfer*, Vol. 7, No. 6, 1967, pp. 891–941. doi:10.1016/0022-4073(67)90005-2

[6] Hoshizaki, H., and Wilson, K. H., "Convective and Radiative Heat Transfer During Superorbital Entry," NASA CR-584, Sept. 1966.

[7] Park, C., "Nonequilibrium Air Radiation (NEQAIR) Program: User's Manual," NASA TM 86707, 1985.

[8] Park, C., "Calculation of Nonequilibrium Radiation in AOTV Flight Regimes," AIAA Paper 84-0306, 1984.

[9] Whiting, E. E., Arnold, J. O., and Lyle, G. C., "A Computer Program for a Line-by-Line Calculation of Spectra from Diatomic Molecules and Atoms Assuming a Voigt Line Profile," NASA TN D-5088, 1969.

[10] Wiese, W. L., Smith, M. W., and Glennon, B. M., *Atomic Transition Probabilities*, Vol. 1, National Bureau of Standards, Rept. NSRDS-NBS 4, Washington, D.C., May 1966.

[11] Griem, H. R., *Spectral Line Broadening by Plasmas*, Academic Press, New York, 1974.

[12] Arnold, J. O., Whiting, E. E., and Lyle, G. C., "Line by Line Calculation of Spectra from Diatomic Molecules and Atoms Assuming a Voight Line Profile," *Journal of Quantitative Spectroscopy and Radiative Transfer*, Vol. 9, No. 6, 1969, pp. 775–798. doi:10.1016/0022-4073(69)90075-2

[13] Chambers, L. H., "Predicting Radiative Heat Transfer in Thermochemical Nonequilibrium Flow Fields," NASA TM-4564, 1994.

[14] Hartung, L. C., "Development of a Nonequilibrium Radiative Heating Prediction Method for Coupled Flowfield Solutions," *Journal of Thermophysics and Heat Transfer*, Vol. 6, No. 4, 1992, pp. 618–625. doi:10.2514/3.11542

[15] Johnston, C. O., "Nonequilibrium Shock-Layer Radiative Heating for Earth and Titan Entry," Ph.D. Dissertation, Virginia Polytechnic and State Univ., Blacksburg, VA, 2006.

[16] Prabhu, R. K., and Erickson, W. D., "A Rapid Method for the Computation of Equilibrium Chemical Composition of Air to 15,000 K," NASA TP-2792, Mar. 1988.

[17] Cunto, W., Mendoza, C., Ochsenbein, F., and Zeippen, C. J."TOPbase at the CDS," *Astronomy and Astrophysics*, Vol. 275, 1993, pp. L5–L8.

[18] Gupta, R. N., Lee, K.-P., Moss, J. N., and Sutton, K., "Viscous Shock-Layer Solutions with Coupled Radiation and Ablation for Earth Entry," *Journal of Spacecraft and Rockets*, Vol. 29, No. 2, 1992, pp. 173–181. doi:10.2514/3.26332

[19] Sutton, K., "Air Radiation Revisited," AIAA Paper 84-1733, 1984.

[20] Gupta, R. N., "Aerothermodynamic Analysis of Stardust Sample Return Capsule with Coupled Radiation and Ablation," *Journal of Spacecraft and Rockets*, Vol. 37, No. 4, 2000, pp. 507–514.

[21] Balakrishnan, A., Park, C., and Green, M. J., "Radiative Viscous Shock-Layer Analysis of Fire, Apollo, and PAET Flight Data," AIAA Paper 85-1064, 1985.

[22] Gupta, R. N., "Navier–Stokes and Viscous Shock-Layer Solutions for Radiating Hypersonic Flows," AIAA Paper 87-1576, 1987.
[23] Tauber, M. E., and Sutton, K., "Stagnation-Point Radiative Heating Relations for Earth and Mars Entries," *Journal of Spacecraft and Rockets*, Vol. 28, No. 1, 1991, pp. 40–42. doi:10.2514/3.26206
[24] Sutton, K., and Hartung, L. C., "Equilibrium Radiative Heating Tables for Earth Entry," NASA TM-102652, 1990.
[25] *NIST Atomic Spectra Database* [online database], http://physics.nist.gov/PhysRefData/ASD/index.html, July 2006 [retrieved 3 Sept. 2006].
[26] Wiese, W. L., Fuhr, J. R., and Deters, T. M., "Atomic Transition Probabilities of Carbon, Nitrogen, and Oxygen," *Journal of Physical and Chemical Reference Data*, Monograph No. 7, 1996; also available online at http://www.nist.gov/srd/PDFfiles/jpcrdM7.pdf.
[27] Moore, C. E., *Tables of Spectra of Hydrogen, Carbon, Nitrogen and Oxygen Atoms and Ions*, edited by J. W. Gallagher, CRC Press, Boca Raton, FL, 1993.
[28] Kelly, R. L., "Atomic and Ionic Spectrum Lines Below 2000 Angstroms: Hydrogen Through Krypton," *Journal of Physical and Chemical Reference Data*, Vol. 16, Supplement 1, 1987; also available online at http://www.nist.gov/srd/PDFfiles/jpcrdS1Vol16.pdf.
[29] Kaufman, V., and Ward, J. F., "Newly Measured and Calculated Wavelengths in the Vacuum Ultraviolet Spectrum of Neutral Nitrogen," *Applied Optics*, Vol. 6, No. 1, 1967, pp. 43–46.
[30] Goldbach, C., Martin, M., Nollez, G., Plomdeur, P., Zimmerman, J.-P., and Babic, D., "Oscillator Strength Measurements in the Vacuum Ultraviolet, 1: The Strong 1243, 1493, 1743 Angstrom Multiplets of Neutral Nitrogen," *Astronomy and Astrophysics*, Vol. 161, No. 1, 1986, pp. 47–54.
[31] Goldbach, C., Ludke, T., Martin, M., and Nollez, G. D., "Oscillator Strength Measurements in the Vacuum Ultraviolet, 5: Neutral Nitrogen Lines in the 950–1200 Angstrom Range," *Astronomy and Astrophysics*, Vol. 266, No. 1, 1992, pp. 605–612.
[32] Goldbach, C., and Nollez, G. D., "Oscillator Strength Measurements in the Vacuum Ultraviolet, 3: Weak Lines of Neutral Nitrogen," *Astronomy and Astrophysics*, Vol. 201, No. 1, 1988, pp. 189–193.
[33] Zhu, Q., Bridges, J. M., Hahn, T., and Wiese, W. L., "Atomic Transition-Probability Measurements for Prominent Spectral Lines of Neutral Nitrogen," *Physical Review A*, Vol. 40, No. 7, 1989, pp. 3721–3726. doi:10.1103/PhysRevA.40.3721
[34] Musielok, J., Wiese, W. L., and Veres, G., "Atomic Transition Probabilities and Tests of the Spectroscopic Coupling Scheme for N I," *Physical Review A*, Vol. 51, No. 5, 1995, pp. 3588–3597. doi:10.1103/PhysRevA.51.3588
[35] *The Opacity Project*, Vol. 1, Inst. of Physics, Philadelphia, 1995.
[36] Hibbert, A., Biemont, E., Godefroid, M., and Vaeck, N., "New Accurate Transition Probabilities for Astrophysically Important Lines of Neutral Nitrogen," *Astronomy and Astrophysics Supplement Series*, Vol. 88, June 1991, pp. 505–524.
[37] Armstrong, B. H., "Apparent Positions of Photoelectric Edges and the Merging of Spectrum Lines," *Journal of Quantitative Spectroscopy and Radiative Transfer*, Vol. 4, No. 1, 1964, pp. 207–214. doi:10.1016/0022-4073(64)90063-9
[38] Hunt, B. L., and Sibulkin, M., "A Simple Method for Calculating the Frequency-Integrated Radiation due to Weak, Closely Spaced Lines in a Uniform Gas," *Journal of Quantitative Spectroscopy and Radiative Transfer*, Vol. 7, No. 6, 1967, pp. 951–964. doi:10.1016/0022-4073(67)90007-6
[39] Wiese, W. L., and Fuhr, J. L., "Improved Critical Compilations of Selected Atomic Transition Probabilities for Neutral and Singly Ionized Carbon," *Journal of Physical and Chemical Reference Data*, Vol. 36, No. 4, 2007, pp. 1287–1345. doi:10.1063/1.2740642
[40] Fischer, C. F., and Tachiev, G., "Breit-Pauli Energy Levels, Lifetimes, and Transition Probabilities for the Berrylliumlike to Neonlike Sequences," *Atomic Data and Nuclear Data Tables*, Vol. 87, No. 1, 2004, pp. 1–184. doi:10.1016/j.adt.2004.02.001
[41] Tayal, S. S., "New Accurate Oscillator Strengths and Electronic Excitation Collision Strengths for N I," *The Astrophysical Journal. Supplement Series*, Vol. 163, Mar. 2006, pp. 207-223. doi:10.1086/499337
[42] Dumont, P. D., Biemont, E., and Grevesse, N., "Transition Probabilities for Vacuum Ultraviolet Lines of N I Through N IV," *Journal of Quantitative Spectroscopy and Radiative Transfer*, Vol. 14, No. 11, 1974, pp. 1127–1141. doi:10.1016/0022-4073(74)90030-2
[43] Hutchinson, R. B., "Radiative Lifetimes of, U. V. Multiplets in Atomic Carbon, Nitrogen, and Oxygen," *Journal of Quantitative Spectroscopy and Radiative Transfer*, Vol. 11, No. 1, 1971, pp. 81–91. doi:10.1016/0022-4073(71)90165-8
[44] Page, W. A., Compton, D. L., Borucki, W. J., Cliffone, D. L., and Cooper, D. M., "Radiative Transport in Inviscid Nonadiabatic Stagnation-Region Shock-Layers," AIAA Paper 68-784, June 1968.
[45] Park, C., "Calculation of Radiation from Argon Shock Layers," *Journal of Quantitative Spectroscopy and Radiative Transfer*, Vol. 28, No. 1, 1982, pp. 29–40. doi:10.1016/0022-4073(82)90094-2
[46] Cowley, C. R., "An Approximate Stark Broadening Formula for Use in Spectrum Synthesis," *Observatory*, Vol. 91, Aug. 1971, pp. 139–140.
[47] Arnold, J. O., Cooper, D. M., Park, C., and Prakash, S. G., "Line-by-Line Transport Calculations for Jupiter Entry Probes," AIAA Paper 79-1082, 1979.
[48] Morris, J. C., and Garrison, R. L., "Measurements of the Radiation Emitted f-Values and Stark Half-Widths for the Strong Vacuum Ultraviolet Lines of O I and N I," *Physical Review*, Vol. 188, No. 1, 1969, pp. 112–118. doi:10.1103/PhysRev.188.112
[49] Helbig, V., Kelleher, D. E., and Wiese, W. L., "Stark Broadening Study of Neutral Nitrogen Lines," *Physical Review A*, Vol. 14, No. 3, 1976, pp. 1082–1093. doi:10.1103/PhysRevA.14.1082
[50] Cullmann, E., and Labuhn, F., "Stark Broadening of Nitrogen (I) Vacuum-U.V. Lines Using a Wall-Stabilized Arc," *Journal of Quantitative Spectroscopy and Radiative Transfer*, Vol. 20, No. 2, 1978, pp. 205–209. doi:10.1016/0022-4073(78)90087-0
[51] Nubbemeyer, H., "Experimental Ion Contributions to the Stark Broadening of Neutral Nitrogen Spectral Lines in the Vacuum UV," *Physical Review A*, Vol. 22, No. 3, 1980, pp. 1034–1040. doi:10.1103/PhysRevA.22.1034
[52] Goly, A., and Weniger, S., "Stark Broadening of Some C (I) and N (I) Vacuum Ultraviolet Lines," *Journal of Quantitative Spectroscopy and Radiative Transfer*, Vol. 36, No. 2, 1986, pp. 147–161. doi:10.1016/0022-4073(86)90117-2
[53] Sohns, E., and Kock, M., "Plasma Diagnostics Based on Self-Reversed Lines, 2: Application to Nitrogen, Carbon, and Oxygen Arc Measurements in the Vacuum Ultraviolet," *Journal of Quantitative Spectroscopy and Radiative Transfer*, Vol. 47, No. 5, 1992, pp. 335–343. doi:10.1016/0022-4073(92)90035-3
[54] Whiting, E. E., "An Empirical Approximation to the Voigt Profile," *Journal of Quantitative Spectroscopy and Radiative Transfer*, Vol. 8, No. 6, 1968, pp. 1379–1384. doi:10.1016/0022-4073(68)90081-2
[55] Olivero, J. J., and Longbothum, R. L., "Empirical Fits to the Voigt Line Width: A Brief Review," *Journal of Quantitative Spectroscopy and Radiative Transfer*, Vol. 17, No. 2, 1977, p. 233. doi:10.1016/0022-4073(77)90161-3
[56] Whiting, E. E., and Park, C., "Radiative Heating at the Stagnation Point of the AFE Vehicle," NASA TM-0102829, 1990.
[57] Kleb, B., and Johnston, C. O., "Uncertainty Analysis of Air Radiation for Lunar Return Shock Layers," AIAA Paper 2008-6388, 2008.
[58] Tannehill, J. C., Anderson, D. A., and Pletcher, R. H., *Computational Fluid Mechanics and Heat Transfer*, Taylor and Francis, Philadelphia, 1997, pp. 334–335.
[59] Liu, Y., Lin, J., Huang, G., Guo, Y., and Duan, C., "Simple Empirical Analytical Approximation to the Voigt Profile," *Journal of the Optical Society of America B (Optical Physics)*, Vol. 18, No. 5, 2001, pp. 666–672. doi:10.1364/JOSAB.18.000666
[60] Lino da Silva, M., "An Adaptive Line-by-Line Statistical Model for Fast and Accurate Spectral Simulations in Low-Pressure Plasmas," *Journal of Quantitative Spectroscopy and Radiative Transfer*, Vol. 108, No. 1, 2007, pp. 106–125. doi:10.1016/j.jqsrt.2007.03.005
[61] Zel'dovich, Y. B., and Raizer, Y. P., *Physics of Shock Waves and High Temperature Hydrodynamic Phenomena*, Vol. 1, Academic Press, New York, 1966, pp. 248–276, 283–298.
[62] Hofsaess, D., "Photoionization Cross-Sections Calculated by Scaled Thomas-Fermi Method ($h\nu < 50$ eV)," *Atomic Data and Nuclear Data Tables*, Vol. 24, No. 4, 1979, pp. 285–321. doi:10.1016/0092-640X(79)90011-1
[63] Biberman, L. M., and Norman, G. E., "Recombination Radiation and Brehmsstrahlung," *Journal of Quantitative Spectroscopy and Radiative Transfer*, Vol. 3, No. 3, 1963, pp. 221–245. doi:10.1016/0022-4073(63)90034-7

[64] Biberman, L. M., and Norman, G. E., "On the Calculation of Photoionization Absorption," *Optics and Spectroscopy (USSR)*, Vol. 8, No. 4, 1960, pp. 230–232.

[65] Norman, G. E., "The Role of the Negative Nitrogen Ion N^- in the Production of the Continuous Spectrum of Nitrogen and Air Plasmas," *Optics and Spectroscopy (USSR)*, Vol. 17, No. 1, 1964, pp. 94–96.

[66] Allen, R. A., and Textoris, A., "Evidence for the Existence of N^- from the Continuum Radiation from Shock Waves," *Journal of Chemical Physics*, Vol. 40, No. 11, 1964, pp. 34–45.

[67] Morris, J. C., Krey, R. U., and Bach, G. R., "The Continuum Radiation of Oxygen and Nitrogen for Use in Plasma Temperature Determination," *Journal of Quantitative Spectroscopy and Radiative Transfer*, Vol. 6, No. 6, 1966, pp. 727–740. doi:10.1016/0022-4073(66)90017-3

[68] Konkov, A. A., Nikolaev, V. M., and Plastinin, Y. A., "On the Intensity of Emission Continuum of the Negative Nitrogen Atom," *Optics and Spectroscopy (USSR)*, Vol. 25, No. 5, 1968, pp. 380–382.

[69] Asinovskii, E. I., Kirillin, A. V., and Kobzev, G. A., "Continuous Radiation of Nitrogen Plasma," *High Temperature*, Vol. 6, No. 4, 1968, pp. 710–712.

[70] Moskvin, Y. V., "Cross-Section Photo-Detachment of the Negative Nitrogen Ion," *Optics and Spectroscopy (USSR)*, Vol. 28, No. 2, 1970, p. 356.

[71] Ciffone, D. L., and Borucki, J. G., "Spectral Measurements of Nitrogen Continuum Radiation Behind Incident Shocks at Speeds up to 13 km/ sec," *Journal of Quantitative Spectroscopy and Radiative Transfer*, Vol. 11, No. 9, 1971, pp. 1291–1310. doi:10.1016/0022-4073(71)90001-X

[72] Cooper, D. M., "Spectral Intensity Measurements from High-Pressure Nitrogen Plasma," *Journal of Quantitative Spectroscopy and Radiative Transfer*, Vol. 12, No. 8, 1972, pp. 1175–1189. doi:10.1016/0022-4073(72)90059-3

[73] D'Yachkov, L. G., Golubev, O. A., Kobzev, G. A., and Vargin, A. N., "Studies of Continuum Radiation from Nitrogen, Oxygen and Carbon Dioxide Plasmas in the Vacuum Ultraviolet Region," *Journal of Quantitative Spectroscopy and Radiative Transfer*, Vol. 20, No. 2, 1978, pp. 175–189. doi:10.1016/0022-4073(78)90085-7

[74] Cooper, D. M., "Equilibrium Air Radiation from Shock Layers at 11.3 km/ sec," *AIAA Journal*, Vol. 4, No. 12, Dec. 1966, pp. 2125–2130. doi:10.2514/3.3865

[75] Barfield, W. D., "Theoretical Study of Equilibrium Nitrogen Plasma Radiation," *Journal of Quantitative Spectroscopy and Radiative Transfer*, Vol. 17, No. 4, 1977, pp. 471–482. doi:10.1016/0022-4073(77)90094-2

[76] Soon, W. H., and Kunc, J. A., "Nitrogen-Plasma Continuum Emission Associated with N-(3P) and N-(1D) ions," *Physical Review A*, Vol. 41, No. 8, 1990, pp. 4531–4533. doi:10.1103/PhysRevA.41.4531

[77] Chauveau, S., Deron, C., Perrin, M.-Y., Riviere, P., and Soufiani, A., "Radiative Transfer in LTE Air Plasmas for Temperatures up to 15,000 K," *Journal of Quantitative Spectroscopy and Radiative Transfer*, Vol. 77, No. 2, 2003, pp. 113–130. doi:10.1016/S0022-4073(02)00080-8

[78] Patch, R. W., Shackleford, W. L., and Penner, S. S., "Approximate Spectral Absorption Coefficient Calculations for Electronic Band Systems Belonging to Diatomic Molecules," *Journal of Quantitative Spectroscopy and Radiative Transfer*, Vol. 2, No. 3, July–Sept. 1962, pp. 263–271. doi:10.1016/0022-4073(62)90002-X

[79] Golden, S. A., "Approximate Spectral Absorption Coefficients of Electronic Transitions in Diatomic Molecules," *Journal of Quantitative Spectroscopy and Radiative Transfer*, Vol. 7, No. 1, 1967, pp. 225–249. doi:10.1016/0022-4073(67)90067-2

[80] Johnston, C. O., Hollis, B. R., and Sutton, K., "Radiative Heating Methodology for the Huygens Probe," *Journal of Spacecraft and Rockets*, Vol. 44, No. 5, 2007, pp. 993–1002. doi:10.2514/1.26424

[81] Laux, C. O., "Optical Diagnostics and Radiative Emission of Air Plasmas," Mechanical Engineering Department, Stanford Univ. Rept. T-288, Stanford, CA, 1993.

[82] Whang, T. J., Guoxing, Z., Stwalley, W. C., and Wu, C. Y. R., "Franck-Condon Factors of the. . .Transitions of N_2," *Journal of Quantitative Spectroscopy and Radiative Transfer*, Vol. 55, No. 3, 1996, pp. 335–344. doi:10.1016/0022-4073(95)00169-7

[83] Stahel, D., Leoni, M., and Dresslar, K., "Nonadiabatic Representations of the $^1\Sigma_u^+$ and $^1\Pi_u$ States of the N_2 Molecule," *Journal of Chemical Physics*, Vol. 79, No. 6, 1983, pp. 2541–2558. doi:10.1063/1.446166

[84] Chauveau, S., Perrin, M. Y., Riviere, P., and Soufiani, A., "Contributions of Diatomic Molecular Electronic Systems to Heated Air Radiation," *Journal of Quantitative Spectroscopy and Radiative Transfer*, Vol. 72, No. 4, 2002, pp. 503–530. doi:10.1016/S0022-4073(01)00141-8

[85] Generosa, J. I., Harris, R. A., and Sullo, L. R., U.S. Air Force Weapons Lab. TR-70-108, Kirtland AFB, NM, 1971.

G. Palmer
Associate Editor